Preparation of $CaAlSiN_3:Eu^{2+}$ Phosphors by the Self-Propagating High-Temperature Synthesis and Their Luminescent Properties

Xianqing Piao,[†] Ken-ichi Machida,*[,†] Takashi Horikawa,[†] Hiromasa Hanzawa,[‡] Yasuo Shimomura,[§] and Naoto Kijima[§]

Center for Advanced Science and Innovation, Osaka University, 2-1 Yamadaoka, Suita, Osaka 565-0871, Graduate School of Engineering Science, Osaka University, 1-3 Machikaneyama-cho, Toyonaka, Osaka 560-8531, and Mitsubishi Chemical Group Science and Technology Research Center, Inc., 1000 Kamoshida-cho, Aoba-ku, Yokohama, Kanagawa 227-8502, Japan

Received March 6, 2007. Revised Manuscript Received May 20, 2007

Divalent europium-doped nitride phosphors, $Ca_{1-x}Eu_xAlSiN_3$ ($x = 0-0.2$), were successfully prepared by the self-propagating high-temperature synthesis (SHS) by using $Ca_{1-x}Eu_xAlSi$ alloy powder as a precursor. The Rietveld refinement analysis was carried out on the $CaAlSiN_3$ host lattice to elucidate the luminescence properties of dopant Eu^{2+} on the tetrahedrally coordinated site. For the Eu^{2+} doped samples, strong absorption peaking at about 460 nm was observed on the excitation spectra, which matched perfectly with the current blue light of InGaN/GaN light-emitting diodes (LEDs). The optimized sample, $Ca_{0.98}Eu_{0.02}AlSiN_3$, gave the red emission peaking at 649 nm of which the intensity was competitive with the sample prepared from the metal nitride raw materials (Ca_3N_2, AlN, Si_3N_4, and EuN). The CIE chromaticity index (0.647, 0.347) with high color saturation indicated that it was a promising candidate as a red-emitting phosphor for the InGaN/GaN-based down-conversion white LEDs for general illumination or displays.

1. Introduction

The white light-emitting diodes (LEDs), featuring the advantages of high light efficiency, low energy consumption, and long service lifetime, have drawn much attention because of their wide applications. Currently, the most common approach to produce white light is to combine a blue LED chip with a yellow phosphor, and some detailed studies on the combination of the InGaN blue-emitting LED and Ce^{3+}-doped yttrium aluminum garnet (YAG) yellow phosphor are presented.[1,2] However, the "white" output light of such an LED is limited with high correlated color temperature (CCT) ranging from 4500 to 11 000 K; that is, the cold white light is usually obtained. To obtain the warm white light output, a complementary red light is necessary to compensate the red color deficiency or to produce white light in the blue-green-red (BGR) mode. For both routes, the red phosphors that can be efficiently excited by the GaN or InGaN LED chip are in great demand.

As the 4f−5d transition of Eu^{2+} ion is sensitive to the crystal field and covalency, the Eu^{2+} doped phosphors have a strong absorption in the UV to the visible spectral region and exhibit broad emission bands covering the color from blue to red. Recently, the Eu^{2+}-activated nitride phosphors have drawn much interest because of their outstanding thermal and chemical stability and interesting photoluminescence properties. These phosphors, such as Eu^{2+}-doped α- and β-SiAlON,[3,4] $M^{II}_2Si_5N_8:Eu^{2+}$ (M^{II} = Ca, Sr, Ba),[5−8] and $LaSi_3N_5:Eu^{2+}$,[9] efficiently emit visible light under the excitation of near-UV or blue light, allowing them to be used as the down-conversion phosphors in the white LEDs. The nitrogen atoms in such nitride hosts are generally connected with two ($N^{[2]}$), three ($N^{[3]}$), or even four ($N^{[4]}$) silicon atoms, such as in $BaYbSi_4N_7$[10] and $BaSi_7N_{10}$.[11] The degree of condensation κ (molar ratio of Si/N) has been observed within the range of 1/2 to 3/4, which is not accessible for oxysilicates (the maximum is 1/2 in SiO_2).[12] These highly condensed SiN_4-based networks guarantee the extraordinary chemical and thermal stability. Furthermore, the activators, such as Eu^{2+} or Ce^{3+}, show interesting luminescent properties in such nitride host as surrounded by the strong covalent

* Corresponding author. Tel.: +81-6-6879-4209. Fax: +81-6-6879-4209. E-mail: machida@casi.osaka-u.ac.jp.
[†] Center for Advanced Science and Innovation, Osaka University.
[‡] Graduate School of Engineering Science, Osaka University.
[§] Mitsubishi Chemical Group Science and Technology Research Center, Inc.

(1) Nakamura, S.; Fasol, G. *The blue Laser Diode: GaN Based Light Emitters and Lasers*; Springer: Berlin, 1997.
(2) Nakamura, S.; Mukai, T.; Senoh, M. *Appl. Phys. Lett.* **1994**, *64*, 1687.
(3) Xie, R. J.; Hirosaki, N.; Sakuma, K.; Yamamoto, Y.; Mitomo, M. *Appl. Phys. Lett.* **2004**, *84*, 5404. Suehiro, T.; Hirosaki; N.; Xie, R.-J.; Mitomo, M. *Chem. Mater.* **2005**, *17*, 308.
(4) Hirosaki, N.; Xie, R.-J.; Kimoto, K.; Sekiguchi, T.; Yamamoto, Y.; Suehiro, T.; Mitomo, M. *Appl. Phys. Lett.* **2005**, *86*, 211905.
(5) Höppe, H. A.; Lutz, H.; Morys, P.; Schnick, W.; Seilmeier, A. *J. Phys. Chem. Solid* **2000**, *61*, 2001.
(6) Li, Y. Q.; van Steen, J. E. J.; van Krevel, J. W. H.; Botty, G.; Delsing, A. C. A.; DiSalvo, F. J.; de With, G.; Hintzen, H. T. *J. Alloys Compd.* **2006**, *417*, 273.
(7) Piao, X. Q.; Horikawa, T.; Hanzawa, H.; Machida, K. *Appl. Phys. Lett.* **2006**, *88*, 161908.
(8) Piao, X. Q.; Horikawa, T.; Hanzawa, H.; Machida, K. *Chem. Lett.* **2006**, *35*, 334.
(9) Uheda, K.; Takizawa, H.; Endo, T.; Yamane, H.; Shimada, M.; Wang, C.-M.; Mitomo, M. *J. Lumin.* **2000**, *87*−*89*, 967.
(10) Li, Y. Q.; de With, G.; Hintzen, H. T. *J. Alloys Compd.* **2004**, *385*, 1.
(11) Huppertz, H.; Schnick, W. *Chem.—Eur. J.* **1997**, *3*, 249.
(12) Hoeppe, H. A.; Stadler, F.; Oeckler, O.; Schnick, W. *Angew. Chem., Int. Ed.* **2004**, *43*, 5540.

10.1021/cm070623c CCC: $37.00
Published on Web 08/11/2007

N^{3-} ions. Very recently, Uheda and co-workers reported $CaAlSiN_3:Eu^{2+}$ as a novel red phosphor for white LED use.[13] The application, however, was limited to some extent because the air-sensitive Ca_3N_2 must be used as a raw material in addition to the inert AlN and Si_3N_4. Thus, the critical preparation condition of high temperature and pressure is necessary to complete the conventional solid-state reaction. Consequently, from the viewpoint of industrial applications, new synthesis routes for the high-performance $CaAlSiN_3:Eu^{2+}$ phosphor are still urgently required.

In the present work, $CaAlSiN_3:Eu^{2+}$ phosphors were synthesized by using self-propagating high-temperature synthesis (SHS) method, which is widely used in the preparation of alloy compounds, borides, or nitrides.[14] The structure, thermal and chemical stability, and luminescent properties of obtained $CaAlSiN_3:Eu^{2+}$ phosphors were investigated as an efficient red phosphor for the white LEDs application.

2. Experimental and Measurement Sections

The $Ca_{1-x}Eu_xAlSi$ alloy powder prepared from silicon shot (Wako, 99.999%), calcium (Nilaco, 99.9%), aluminum (Nilaco, 99.99%), and europium (Wako, 99.99%) metal shots was used as precursors for synthesizing the $CaAlSiN_3:Eu^{2+}$ phosphors. These raw materials were arc-melted several times in an Ar atmosphere to form the homogeneous alloy ingot that was easily grounded to fine powder. The weight loss during the arc melting was less than 1 wt %. The fine alloy powder was transferred to a Mo boat and then loaded into a radio frequency (RF) furnace (ZrB_2 heater). The heating chamber was pumped down, and back filled with high purity N_2 (6 N), and heated under continuous N_2 flow with a rate of 20 mL/min. The temperature was slowly (10 °C/min) increased up to 1050 °C at which the SHS occurred, and then the product after the SHS process was calcined at 1450−1550 °C for 6 h for further nitridation. At last, the power was switched off and the samples were cooled to room temperature with the furnace.

The samples were identified by X-ray powder diffraction (RINT2200, Rigaku) with Cu Kα radiation operating at 40 kV and 30 mA. The data for Rietveld analysis were collected with a step of 0.01° (2θ) and a scanning speed of 0.5°/min in the range of 10−90°. The powder was mounted on a flat plate holder by the side filling method to avoid the preferred orientation. The oxygen content was measured by an O/N analyzer (EMGA-550, Horiba). Diffuse reflection spectra were obtained by a $BaSO_4$ powder calibrated UV−vis spectrophotometer (UV-2200, Shimadzu). The photoluminescence spectra were measured using fluorescent spectrophotometers (Hitachi F-4500) at room-temperature equipped with a Xe lamp as an excitation source and USB Ocean 2000 (Ocean Optics) fixed on a liquid helium cooled cryostat in the range of 5−280 K).

3. Results and Discussion

Figure 1 shows the X-ray diffraction (XRD) pattern of the CaAlSi alloy precursor powder. The CaAlSi intermetallic compound, which is isostructural with MgB_2 (AlB_2 type C_{32} crystal structure), is generally known as a superconductor.

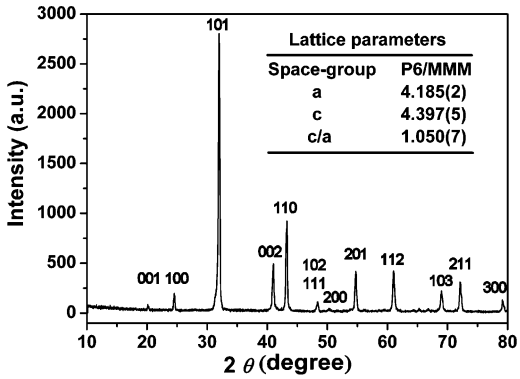

Figure 1. XRD pattern of CaAlSi alloy powder precursor; the inset table shows the calculated lattice parameters.

The lattice parameters are calculated using the TREOR 90 version of the indexing program TREOR,[15] and the obtained parameters (listed in the inset of Figure 1) are in good agreement with the previous work.[16] The successful ignition at about 1050 °C leads to the propagation of a flame to the whole sample area, and the local temperature is observed around 1900 °C because the SHS is an exothermal process and then reverts to the furnace temperature. The reaction is simply expressed as follows:

$$2Ca_{1-x}Eu_xAlSi + 3N_2 \rightarrow 2Ca_{1-x}Eu_xAlSiN_3 \quad (x = 0-0.2) \tag{1}$$

Of course, the contribution of the solid-state reaction of the corresponding nitrides (Ca_3N_2, AlN, Si_3N_4) that nitrified from the precursor to form the $Ca_{1-x}Eu_xAlSiN_3$ compound cannot be ruled out. After the SHS process occurs, further conversion to nitride continues apparently at higher temperature (up to 1500 °C), and the $CaAlSiN_3:Eu^{2+}$ nitride products with carmine color are finally obtained. As the pure metals are used as raw materials to synthesize $Ca_{1-x}Eu_xAlSiN_3$ phosphors, the oxygen content of the resultant sample is suppressed as low as possible. For example, the oxygen content of a typical sample, $Ca_{0.98}Eu_{0.02}AlSiN_3$, is successfully lowered to less than 0.6 wt %, and the measured nitrogen content (29.1 wt %) is close to the stoichiometric value (30.1 wt %), indicating that the alloy precursor is completely nitrified. Figure 2 shows electron microscope images of a typical alloy powder precursor ($Ca_{0.98}Eu_{0.02}AlSi$) and the corresponding phosphor ($Ca_{0.98}Eu_{0.02}AlSiN_3$). The mean size of the precursor is about 1 μm, and the phosphor obtained by the SHS route contains irregular particles with the size of about 6−9 μm, which is larger than that reported in ref 13. In addition, as the exothermal SHS process stimulates the particle coarsening and agglomerating, some larger aggregates (as marked in Figure 2b) are observed even after regrinding in a mortar. Though the uniform morphology is not obtained by this route, it is acceptable for the white LED application as the particle size requirement is not so strict as that in the plasma display panel (PDP) field.

To investigate the crystal structure of the host matrix, the Rietveld refinement analysis is carried out on the undoped

(13) Uheda, K.; Hirosaki, N.; Yamamoto, Y.; Naito, A.; Nakajima, T.; Yamamoto, H. *Electrochem. Solid-State Lett.* **2006**, *9*, H22. Uheda, K.; Hirosaki, N.; Yamamoto, H. *Phys. Status Solidi A* **2006**, *203*, 2712.
(14) Merzhanov, A. G.; Rogachev, A. S. *Pure Appl. Chem.* **1992**, *64*, 941.
(15) Werner, P. E.; Eriksson, L.; Westdahl, M. *J. Appl. Crystallogr.* **1985**, *18*, 367.
(16) Imai, M.; Nishida, K.; Kimura, T.; Abe, H. *Appl. Phys. Lett.* **2002**, *80*, 1019. Sparta, K. M.; Mueller, R.; Merz, M.; Roth, G.; Adelmann, P.; Wolf, T. *Acta Crystallogr., Sect. B* **2006**, *62*, 710.

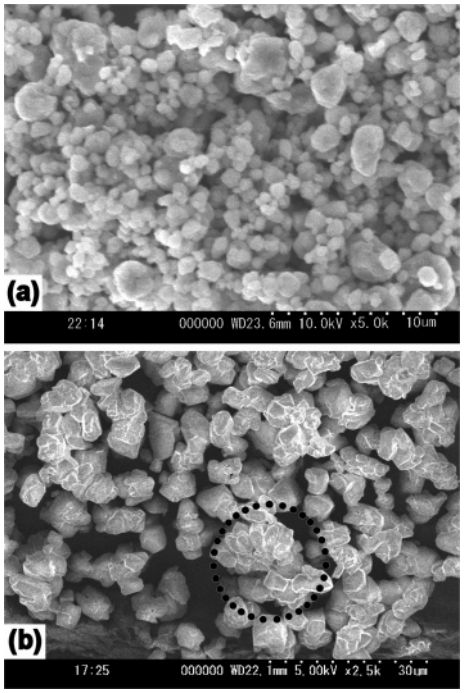

Figure 2. SEM images of $Ca_{0.98}Eu_{0.02}AlSi$ and the corresponding $Ca_{0.98}Eu_{0.02}AlSiN_3$ phosphor.

$CaAlSiN_3$. The XRD pattern of $CaAlSiN_3$ is indexed with the TREOR 90 program package, and the calculation reveals that this compound is attributed to the orthorhombic system. The space group determination is performed with the CHECKCELL[17] program. With regard to the symmetry and space group of the initial compound, two space groups, $Cmc2_1$ and *Cmcm*, are given as the best solutions. On the basis of the presented group−subgroup connection analysis of such AB_2X_3 compound according to Bärnighausen's procedure,[18] the space group of $Cmc2_1$ is chosen for further calculations. For the Rietveld refinement of $CaAlSiN_3$, the atomic coordinates of $NaSi_2N_3$[19] are employed as the starting model, and the structure is refined with the software package of FULLPROF SUITE.[20] Figure 3 shows the comparison of the calculated and observed $CaAlSiN_3$ patterns as well as the difference curve between them. The resultant crystallographic data and atomic coordinates are summarized in Table 1, and these data agree well with the work of Uheda's group.[13] The space group of $Cmc2_1$ is the maximum nonisomorphic subgroup of the ZnO type wurtzite group $P6_3mc$. According to refinement results of the unit cell parameters, the $CaAlSiN_3$ compound presents a normal tetrahedral structure related to the wurtzite type

$$a_0 \sim 3a_w, \quad b_0 \sim \sqrt{3}a_w, \quad c_0 \sim c_w \tag{2}$$

The degree of matching can be evaluated by the ratio of $\epsilon = 2c_0/(a_0/3 + b_0/\sqrt{3})$, and the calculated value ($\epsilon = 1.553$) is close to the ideal quotient (ϵ: $2\sqrt{2}/\sqrt{3} = 1.633$).[21]

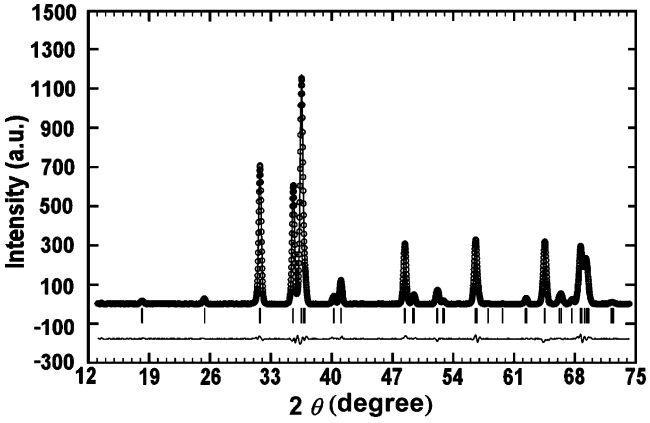

Figure 3. Observed (circle) and calculated (line) X-ray powder diffraction patterns of $CaAlSiN_3$ as well as the difference profile (bottom line) between them. Bragg reflection peak positions are shown as vertical bars.

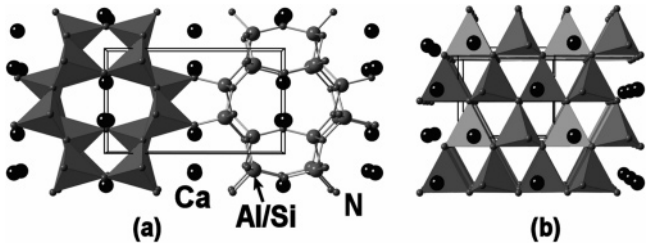

Figure 4. Crystallographic structure of $CaAlSiN_3$ along the (a) [001] (on the left side a polyhedral view of the structure and on the right a ball-stick representation) and (b) [100] directions.

Table 1. Refined Structural Parameters, Atomic Coordinates, Isotropic Displacement Parameters, and Selected Interatomic Distances of $CaAlSiN_3$ Obtained from the Rietveld Refinement Using Powder XRD Data

atom (site)	*x*	*y*	*z*	occupancy	U_{iso} [Å^2]
Ca (4a)	0	0.3156	0.9752	1	0.0167
Al/Si (8b)	0.1714	0.8426	0.0489	1	0.0035
N1 (8b)	0.2123	0.8731	0.4067	1	0.0003
N2 (4a)	0	0.2305	0.5000	1	0.0003

$CaAlSiN_3$		selected distances and angles			
formula weight	137.16	$Ca-N1^I$	2.3995	$N1^I-Ca-N1^{II}$	118.896
crystal system	orthorhombic	$Ca-N1^{II}$	2.3995	$N1^I-Ca-N2^I$	98.984
space group	$Cmc2_1$ (No. 36)	$Ca-N2^I$	2.4433	$N1^I-Ca-N2^{II}$	115.529
cell parameters	$a = 9.731(1)$ Å	$Ca-N2^{II}$	2.5637	$N1^{II}-Ca-N2^I$	98.984
	$b = 5.640(8)$ Å			$N1^{II}-Ca-N2^{II}$	115.529
	$c = 5.041(7)$ Å			$N2^I-Ca-N2^{II}$	104.133
volume	268.72 Å^3	M^a-N1^I	1.7357	$N1^I-M-N1^{II}$	107.628
Z	4	$M-N1^{II}$	1.8009	$N1^I-M-N1^{III}$	104.888
density (calcd)	3.7919 g/cm^3	$M-N1^{III}$	1.8096	$N1^I-M-N2$	111.570
R factors	$R_p = 5.49\%$	M−N2	1.8556	$N1^{II}-M-N1^{III}$	108.249
	$R_{wp} = 9.86\%$			$N1^{II}-M-N2$	112.626
				$N1^{III}-M-N2$	111.493

[a] M = Al/Si.

As shown in Figure 4, the structure of $CaAlSiN_3$ is built up of an MN_4 tetrahedra (M = Al/Si) linked three-dimentional structure: one-third of the nitrogen atoms (N2) are linked with two M neighbors, and the other two-thirds (N1) are connected with three M neighbors. The Al and Si atoms are randomly distributed on the same tetrahedral sites and connected with N atoms to form the vertex-linked M_6N_{18} rings. Very similar ring structures have also been observed in other nitridosilicates, such as $M^{II}_2Si_5N_8$ (M^{II} = Ca, Sr,

(17) Laugier, J.; Bochu, B. *CHECKCELL*: *A Software Performing Automatic Cell/Space Group Determination*; Laboratory of Materials and Phyisical Engineering, School of Physics, University of Grenoble, France, 2000 (http://www.ccp14.ac.uk/tutorial/lmgp/).
(18) Baur, W. H.; McLarnan, T. J. *J. Solid State Chem.* **1982**, *42*, 300.
(19) Jacobs, H.; Mengis, H. *Eur. J. Solid State Inorg. Chem.* **1993**, *30*, 45.
(20) Roisnel, T.; Rodríguez-Carvajal, J. *Mater. Sci. Forum* **2001**, *378−381*, 118.
(21) Guyader, J.; L'Haridon, P.; Laurent, Y.; Jacquet, R.; Roult, G. *J. Solid State Chem.* **1984**, *54*, 251.

Table 2. Lattice Constants of Structurally Related Compounds with $CaAlSiN_3$

	a (Å)	*b* (Å)	*c* (Å)
$LiSi_2N_3$	9.186(3)	5.302(2)	4.776(2)
$NaSi_2N_3$	9.468(1)	5.502(1)	4.878(5)
$NaGe_2N_3$	9.8662(15)	5.7830(9)	5.1221(5)
Si_2N_2O	8.866(2)	5.486(1)	4.845(1)
Si_2N_2NH	9.1930(7)	5.4069(4)	4.8190(4)
Si_2N_2NCN[a]	13.58	5.44	4.81

[a] Belongs to the space group of *Aba*2, while the other five compounds belong to $Cmc2_1$.

Ba).[22] In $CaAlSiN_3$, however, such condensed M_6N_{18} rings are highly oriented with all of the MN_4 tetrahedrons pointing along the [001] direction. By observing along the [100] direction horizontally, two layers with the sequence of CDCD... are found. The layers C and D are topologically identical, and one layer can be regarded as the 180° rotation in *XY* plane of the other. According to the analysis of interatomic distance, the mean distance of M−N is 1.800-(5) Å, and the M−N1 is shorter than that of M-N2. This indicates that threefold bridged N1 contributed dominantly to the rigidness of the structure. Furthermore, in other compounds sharing the isotropic or similar space groups, the N2 sites can be replaced by other anion or anion group such as O^{2-}, NH^{2-}, and $-N=C=N-^{2-}$.[19,21,23−26] As the comparison of unit cell parameters of such compounds (Table 2), the expansion or shrinkage of unit parameters is found to be significantly obvious for the parameter *a* as the Si−N2−Si extends at [100] direction.

Calcium atoms are arranged in the channels formed by Si_6N_{18} rings along [001] orientation. The cation radii of Ca^{2+}, Al^{3+}, and Si^{4+} are considered, combined with the interatomic distances of Ca−N and M−N listed in Table 1, the larger Eu^{2+} ions are assumed to be incorporated into the Ca^{2+} site when $CaAlSiN_3$ is used as a phosphor host. The substitution of the Ca^{2+} ion by the larger Eu^{2+} ion results in the lattice expansion, which is confirmed by the shift of XRD peaks of $Ca_{1-x}Eu_xAlSiN_3$ toward the low 2θ angle side with increasing Eu^{2+} content. The solid solution of Eu^{2+} in $Ca_{1-x}Eu_xAlSiN_3$ is limited to about 20 atom %, and the higher doping concentration of Eu^{2+} ions results in the formation of impurity phases, such as $Eu_2Si_5N_8$ (JCPDS 87-0423). Furthermore, as the cation radii of Eu^{2+} and Sr^{2+} are very close to each other, the latter ion is expected to have a similar solid solution capacity in the $CaAlSiN_3$ host lattice to form $(Ca,Sr)AlSiN_3$ solid solution. Thus, the fine color tuning is expected by changing the crystal field strength. The study from this aspect is still in progress, and the result will be the subject of another publication.

Figure 5 shows the optical reflection spectra of undoped and Eu^{2+}-doped $CaAlSiN_3$. For the undoped sample, which shows pure white body color, a strong absorption shows up

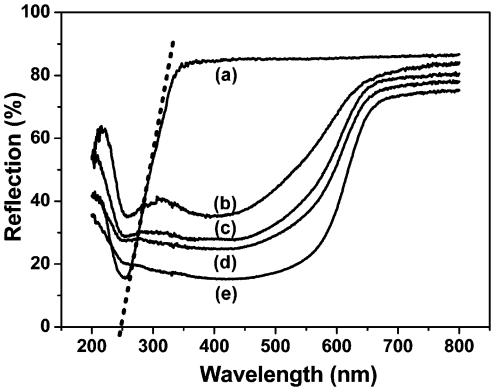

Figure 5. Diffuse reflection spectra of undoped $CaAlSiN_3$ host (a) and $Ca_{1-x}Eu_xAlSiN_3$ samples with $x = 0.02$ (b), 0.05 (c), 0.1 (d), and 0.2 (e).

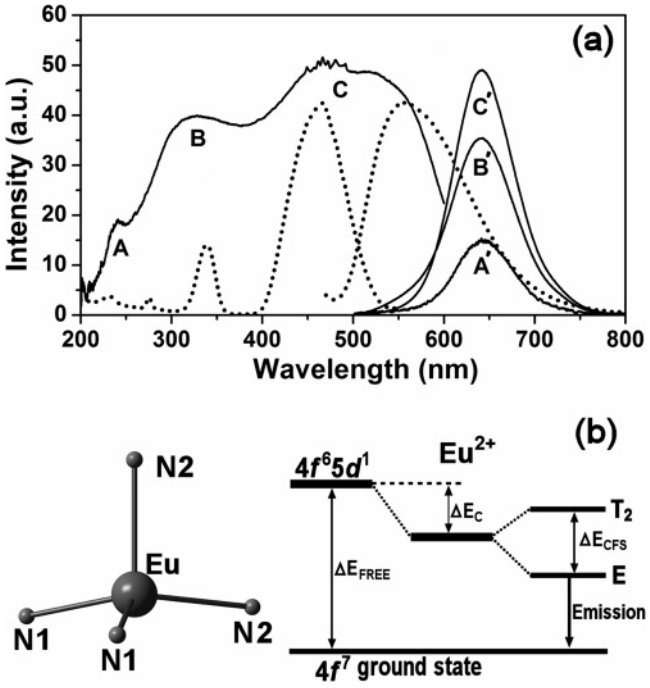

Figure 6. Typical photoluminescence excitation ($\lambda_{mon} = 649$ nm) and emission ($\lambda_{ex} = 460$ nm) spectra of $Ca_{0.98}Eu_{0.02}AlSiN_3$ (a) and the schematic picture of the influence of the environment of a Eu^{2+} on the positions of electronic states (b).

in the range of 200−300 nm caused by the electronic transition of the host. The optical band gap E_g of $CaAlSiN_3$ determined by extrapolating the linear portion of the reflection curve onto energy (wavelength) is about 5.0−5.2 eV. For the Eu^{2+}-doped samples, strong absorption bands are presented in the range of the UV to visible spectral region, which can be assigned to the $4f^7 \rightarrow 4f^65d$ transition of the Eu^{2+} ion. With increasing Eu^{2+} ion concentration, the absorption becomes stronger and the absorption edges shift to the longer wavelength side so that the body color of phosphors reddens gradually.

The room-temperature excitation and emission spectra of $Ca_{0.98}Eu_{0.02}AlSiN_3$ are depicted in Figure 6a. The excitation spectrum is consistent with the corresponding reflection spectrum and shows a broadband covering the region from the near-UV to visible part. The first band located at about 240 nm is caused by the electronic transition between the valence and the conduction band of the $CaAlSiN_3$ host (in accordance with the optical band gap given in Figure 5).

(22) Schlieper, T.; Schnick, W. *Z. Anorg. Allg. Chem.* **1995**, *621*, 1037. Schlieper, T.; Milius, W.; Schnick, W. *Z. Anorg. Allg. Chem.* **1995**, *621*, 1380.
(23) Jean, D.; Yves, L.; Jean-P, C.; Jean, L. *Bull. Soc. Fr. Mineral. Cristallogr.* **1973**, *96*, 21.
(24) Srinivasa, S. R.; Cartz, L.; Jorgensen, J. D.; Worlton, T. G.; Beyerlein, R. A.; Billy, M. *J. Appl. Crystallogr.* **1977**, *10*, 167.
(25) Peters, D.; Jacobs, H. *J. Less-Common Met.* **1989**, *146*, 241.
(26) Riedel, R.; Greiner, A.; Miehe, G.; Dressler, W.; Fuess, H.; Bill, J.; Aldinger, F. *Angew. Chem., Int. Ed. Engl.* **1997**, *36*, 603.

Another two peaking at 320 and 470 nm are due to the excitation of the Eu^{2+} ions ($4f^7 \rightarrow 4f^6 5d$). The 5d levels of Eu^{2+} ions that are not shielded completely by the outer environment split under various ligand field strength, and the number of split levels is determined by the local symmetry around the Eu^{2+} ions. For example, in some compounds with O_h symmetry, the 5d orbitals of Eu^{2+} are split into two levels, T_{2g} and E_g.[27] In the present case, the incorporated Eu^{2+} ions are tetrahedrally coordinated and presented as a EuN_4 tetrahedron that is very rarely observed. According to the interatomic distances listed in Table 1, the calcium atoms are not located exactly in the center of the tetrahedron but moved to the base, and hence a slightly distorted T_d site symmetry is preferred over the other symmetry groups. The 5d orbitals of Eu^{2+} in such an environment are inclined to be separated as T_2 and E levels. In such a model, the energy transition from the ground state ($^8S_{7/2}$) to the barycenters of T_2 and E levels are estimated around 3.75 and 2.41 eV, from the bi-Gaussian fitting of the two excitation bands of the Eu^{2+} ions on an energy scale, respectively. By considering the slightly distorted T_d site symmetry, the energy difference between the T_2 barycenter and the 5d centroid is 1.5 times that between the *E* barycenter and the 5d centroid.[28] The location of the energy centroid of the Eu^{2+} 5d orbitals is evaluated about 3.23 eV above the ground state.

The broad emission bands for all $Ca_{1-x}Eu_xAlSiN_3$ samples are assigned to the allowed $4f^6 5d \rightarrow 4f^7$ transition of Eu^{2+} ions. The sharp characteristic line emission peaks due to $^5D_0 \rightarrow {}^7F_J$ transitions of Eu^{3+}, which locate from 580 to 630 nm, are not observed even in a phosphorescence mode. In fact, the presence of the N^{3-} ion as the anionic netformer in crystals or glasses gives the reducing potential according to[29] $6Eu^{3+} + 2N^{3-} \rightarrow 6Eu^{2+} + 2N_2$. Therefore, only the divalent Eu^{2+} emission is observed in $Ca_{1-x}Eu_xAlSiN_3$ phosphors even though the Eu_2O_3 oxide is used for the conventional solid-state reaction from nitride raw materials (Ca_3N_2, AlN, Si_3N_4). Compared with Eu^{2+}-doped alkaline earth oxyhalides or oxysilicates, the emission of $Ca_{1-x}Eu_xAlSiN_3$ occurs at a fairly long wavelength range. As shown in Figure 6b, the emission of Eu^{2+} is mainly determined by two factors: the shift of the energy centroid (E_C) and effect of crystal field splitting (E_{CFS}). The crystal-field splitting is roughly estimated to be around 1.34 eV from the shape of excitation band, and this value is comparable with other Eu^{2+} doped counterparts.[30] Therefore, the long-wavelength emission (E_{em} = 1.91 eV) is ascribed to the low electronegativity of N^{3-} and high covalency of the Eu−N bond (nephelauxetic effect), which effectively lowers the energy centroid of 5d orbitals of Eu^{2+}. This is supported by the result of solid-state reaction synthesis of the nominal $Ca_{1-x}Eu_xAlSiN_3$ from the raw materials of Ca_3N_2, AlN, and Si_3N_4 which contain some oxygen content. At the same Eu^{2+} concentration, the emission peak blueshifts about 10−20 nm compared with the samples prepared by the SHS route. For the 2 atom % Eu^{2+}-doped sample containing 3.6 wt % of oxygen content, the emission occurs at 631 nm, and the blue wing extends to the short wavelength part (Figure 7). This means that, by incorporating oxygen content, the N2 sites in the EuN_4 tetrahedrons are partially replaced by O^{2-} ions to form EuN_3O, which reduces the nephelauxetic effect around the Eu^{2+} ions and accounts for the blueshift of the emission band. The emission band is originated from the overlap of two types of Eu^{2+} ions with different environments, and it can be separated on an energy scale by bi-Gaussian fitting to two bands peaking at 1.92 eV (646 nm) and 2.04 eV (607 nm). Whereas for the emission band of $Ca_{0.98}Eu_{0.02}AlSiN_3$ obtained by SHS synthesis, only single Gaussian fitting is achieved, and the full width at half-maximum (fwhm) of 75 nm is also less than 90 nm for the high oxygen content sample from the solid-state reaction. On the basis of our previous work,[7] the charge imbalance caused by the substitutional O_N is compensated by the ion vacancy (V_{Ca}) induced by the evaporation of Ca^{2+} at high temperature.

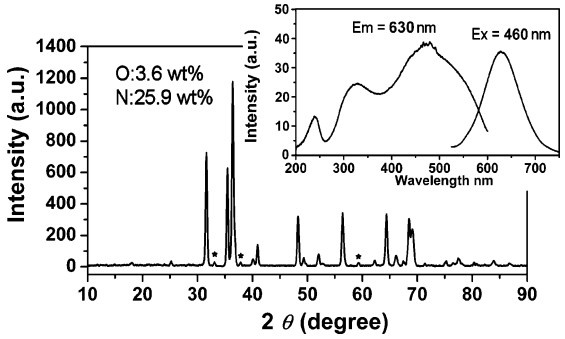

Figure 7. XRD pattern and photoluminescence spectra (inset) of the nominal $Ca_{0.98}Eu_{0.02}AlSiN_3$ sample synthesized from the Ca_3N_2−AlN−Si_3N_4 solid-state reaction.

By exciting at different wavelengths (239, 320, and 470 nm), the emission bands peaking at 649 nm show no shift (emission of A′, B′, and C′ in Figure 6a), which is consistent with the fact that there is only one Ca^{2+} site that can be substituted by the Eu^{2+} activator. The Stokes shift (ΔS) is estimated to be 0.27 ± 0.02 eV by using an almost mirror-image relationship between the emission and the excitation spectra.[31] The transition energy from the $4f^7$ ground state to the $4f^6 5d$ excited-state for Eu^{2+} is lowered from that of the free ion when it is incorporated into a crystal environment. The relationships are described by Dorenbos as[30]

$$E_{em} = E_{free} - D - \Delta S; \quad E_{abs} = E_{free} - D \qquad (3)$$

where E_{free} is the energy difference for the Eu^{2+} ion in the gaseous state and *D* is defined as energy lowering or redshift. The knowledge of E_{em} and ΔS allow us to determine the redshift *D* of the f−d transition in relation to the free Eu^{2+} ion (E_{free} = 4.19 eV) in $Ca_{0.98}Eu_{0.02}AlSiN_3$. The parameter *D* in our case is calculated to be 2.01 ± 0.02 eV and larger than most of the metal nitride phosphors. This is due to, on one hand, the high rigidness of the networks of $CaAlSiN_3$ in which two-thirds of the N ions are threefold linked.

(27) Aull, B. F.; Jenssen, H. P. *Phys. Rev. B* **1986**, *34*, 6640.
(28) Cotton, F. A. *Chemical Applications of Group Theory*; Wiley-Interscience: New York, 1990.
(29) Marchand, R.; L'Haridon, P.; Laurent, Y. *J. Solid State Chem.* **1978**, *24*, 71. de Graaf, D.; Hintzen, H. T.; Hampshire, S.; de With, G. *J. Eur. Ceram. Soc.* **2003**, *23*, 1093.
(30) Dorenbos, P. *J. Lumin.* **2003**, *104*, 239.
(31) Meijerink, A.; Blasse, G. *J. Lumin.* **1989**, *43*, 283.

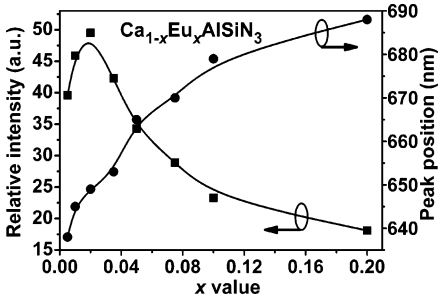

Figure 8. Dependence of emission intensity and peak position of $Ca_{1-x}Eu_xAlSiN_3$ phosphors on Eu^{2+} content.

Consequently, high covalency around the Eu^{2+} activator is expected. On the other hand, the extension of the *E* levels of Eu^{2+} ion in T_d symmetry to the lower energy part also contributes to the larger *D* value. As the redshift coefficient *D* can be regarded as a sum of the lowering of the 5d states centroid and crystal field splitting, the larger *D* accounts for the longer emission of Eu^{2+} in $CaAlSiN_3$ than in the other nitride hosts, such as $CaSiN_2$[32] or $Sr_2Si_5N_8$,[6−8] which give the band emission peak at 605 and 620 nm, respectively.

Dependence of the peak position and emission intensity on Eu^{2+} ion concentration is shown in Figure 8. Obviously, the strong absorption with increasing Eu^{2+} concentration (see Figure 5) does not always favor the elevation of the emission intensity. In $Ca_{1-x}Eu_xAlSiN_3$, the emission intensity is maximized at around 2 atom % of Eu^{2+} ion dopant concentration. The slightly higher critical Eu^{2+} concentration than that in the previously work[13] (1.6 atom %) is possibly due to the evaporation of Eu metal during the high-temperature SHS process. The decrease in the emission intensity beyond a critical concentration is ascribed to the concentration quenching effect that is mainly caused by the energy transfer between two Eu^{2+} ions. Because the $4f^6 5d \rightarrow 4f^7$ transition of the Eu^{2+} ion is allowed as well as the excitation and emission band overlap at 550−630 nm, the energy transfer may occur as a result of multipolar interaction and radiation reabsorption.[33] At the same time, the emission peak position of $Ca_{1-x}Eu_xAlSiN_3$ phosphors shifts from 640 to 690 nm by increasing the Eu^{2+} content. Interestingly, the redshifting behavior is in contradiction with the observation of expansion of crystal lattices which should shift the $4f^6 5d \rightarrow 4f^7$ emission of Eu^{2+} to the high-energy side by decreasing the crystal field strength. This is temporarily contributed to the same reason for the redshifting behavior of Eu^{2+} ions in (Ca, Eu)S and (Sr, Eu)S phosphors.[13,34] According to the recent work of Sakuma et al.,[35] however, it is easily understood by the reabsorption mechanism as in Eu^{2+}-activated Ca-α-SiAlON. With increasing the Eu^{2+} concentration, the excitation edge (550−600 nm) extends significantly to the longer wavelength side (consistent with Figure 5), and then the reabsorption reduces the high-energy portion of the emission band, while the long wavelength part gains intensity. Consequently, the reabsorption derived by the energy transfer results in the redshifting of the emission band.

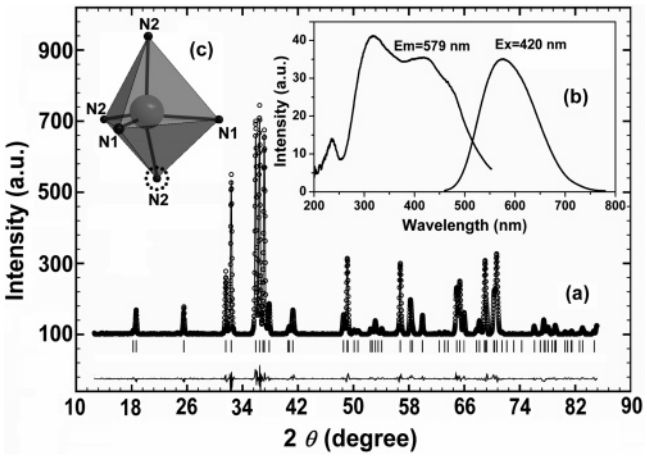

Figure 9. Rietveld refinement analysis (a), photoluminescence spectra (b), and crystallographic environments around Eu^{2+} ions of annealed $Ca_{0.98}Eu_{0.02}AlSiN_3$ phosphor.

Table 3. Rietveld Refinement Result of the Annealed $CaAlSiN_3$ Host

atom (site)	*x*	*y*	*z*	Occupancy	U_{iso} [Å^2]
Ca (4a)	0	0.3494	0.9200	0.9128	0.0545
Al/Si (8b)	0.1743	0.8512	−0.0364	1	0.0212
N1 (8b)	0.2269	0.8668	0.3284	1	0.0046
N2 (4a)	0	0.2350	0.4082	0.901	0.1422
O (4a)	0	0.2350	0.4082	0.099	0.1422

$Ca_{0.913}AlSiN_{2.901}O_{0.099}$		selected distances and angles			
formula weight	133.88	Ca−N1^{I}	2.5203	N1^{I}−Ca−N1^{II}	117.559
cell parameters	$a = 9.499(5)$ Å	Ca−N1^{II}	2.5203	N1^{I}−Ca−N2^{I}	92.926
	$b = 5.659(6)$ Å	Ca−N2^{I}	2.3532	N1^{I}−Ca−N2^{II}	118.733
	$c = 4.998(2)$ Å	Ca−N2^{II}	2.5243	N1^{II}−Ca−N2^{I}	92.926
R_p (%)	9.01			N1^{II}−Ca−N2^{II}	118.733
R_{wp} (%)	14.1			N2^{I}−Ca−N2^{II}	106.308

In addition to studying the activator concentration effect on the emission of the red phosphor, the postannealing effect is also investigated. Generally, the annealing treatment will enhance the emission intensity by improve the crystallinity of the phosphors. In our case, however, the structure distortion is observed unexpectedly by the annealing of the as-prepared samples at 1700 °C for 6 h under 0.2 MPa N_2. The Rietveld refinement for the host is carried out on the same space group ($Cmc2_1$) as that shown in Figure 9a, and the result is listed in Table 3. The obtained XRD pattern is well indexed to the JCPDS card 39-0747, which is found as $CaAlSiN_3$ in $CaO-AlN-Si_3N_4$ by Huang et al.[36] The occupancy of the Ca site is refined as 0.913, and when combined with the measured oxygen content of 1.2 wt %, the chemical composition is expressed as $Ca_{0.913}AlSiN_{2.901}O_{0.099}$ for the annealed host. The lattice constants are somewhat smaller than those of the as-prepared $CaAlSiN_3$, which can be ascribed to the formation of the vacancy on Ca sites during high-temperature annealing. Additionally, the photoluminescence properties of the annealed sample deviate interestingly from the corresponding $Ca_{0.98}Eu_{0.02}AlSiN_3$ phosphor (as-prepared). As shown in Figure 9b, the emission occurs at the much higher energy side (579 nm), and the excitation band gets narrowed compared with the as-prepared one. If

(32) Le Toquin, R.; Cheetham, A. K. *Chem. Phys. Lett.* **2006**, *423*, 352.
(33) Blasse, G. *Phys. Status Solidi B* **1973**, *55*, K131. Blasse, G. *J. Solid State Chem.* **1986**, *62*, 207.
(34) Kaneko, Y.; Koda, T. *J. Cryst. Growth* **1988**, *86*, 72. Kaneko, Y.; Morimoto, K.; Koda, T. *Ouyoubutsuri* **1981**, *50*, 289 (in Japanese).
(35) Sakuma, K.; Hirosaki, N.; Xie, R.-J. *J. Lumin.* **2007**, *126*, 843.
(36) Huang, Z. K.; Sun, W. Y.; Yan, D. S. *J. Mater. Sci. Lett.* **1985**, *4*, 255.

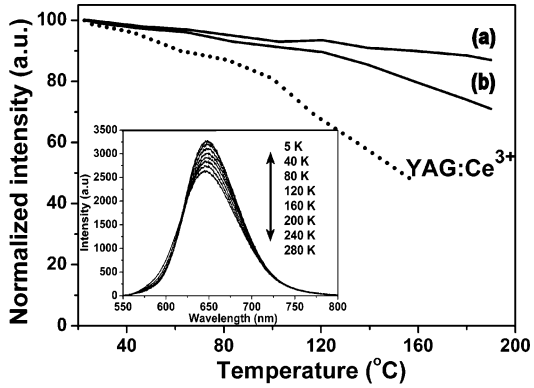

Figure 10. The temperature-dependent emission intensity of $Ca_{1-x}Eu_xAlSiN_3$ samples with $x = 0.02$ (a) and 0.05 (b), and the inset shows the low-temperature emission of $Ca_{0.98}Eu_{0.02}AlSiN_3$.

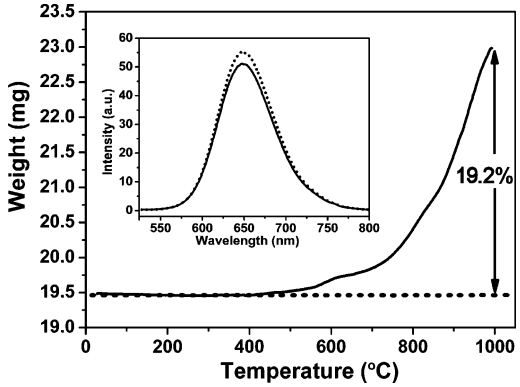

Figure 11. TG curve of $Ca_{0.98}Eu_{0.02}AlSiN_3$ and (inset) the comparison of emission intensity for the same sample before (solid line) and after (dotted line) the acid process.

only four nearest N^{3-} are considered, the mean distance of Ca−N bonds in the annealed sample is 2.4795 Å, and it is larger than that in the as-prepared one (2.4515 Å). A weaker crystal field strength, which is inversely proportional to R^5 (R: chemical bond length between a cation with d orbital electrons and the coordinating anion),[37] is expected for the annealed sample. Induced by the lattice shrinkage, the Ca ion moves further to the bottom of the tetrahedron and almost locates in the N1−N1−N2 plane (Figure 9c). This is in accordance with the refinement of angles listed in Table 3. In this case, the fifth coordinated N^{3-} ion ($d_{Ca-N} = 2.638$) has to be taken into account. Therefore, the variation of the surrounding environment of doped Eu^{2+} ions results in the narrowing of the excitation band and high-energy emission for the annealed sample. Though this annealed phosphor cannot be efficiently excited at 460 nm, its strong absorption in the range of 380−420 nm indicates the application by combining with another type 405 nm blue LED chip.

In the white LED application, a low-temperature quenching effect is in favor of keeping the chromaticity and brightness of white light output. The temperature-dependent emission intensity of the optimized $Ca_{0.98}Eu_{0.02}AlSiN_3$ sample is shown in Figure 10. As the temperature increases from 5 to 280 K, the emission band peaking at 649 nm keeps the position, and the intensity is decreased by 17% of the initial value. With heating the samples up to 150 °C at which the white LEDs usually work, the emission intensity of $Ca_{0.98}Eu_{0.02}AlSiN_3$ and $Ca_{0.95}Eu_{0.05}AlSiN_3$ remains at about 90% and 83% of that measured at room temperature, while at about 60% for the YAG:Ce^{3+} (P46−Y3) phosphor. The widely accepted mechanism for the thermal quenching is the electronic transition through the intersection between the $4f^6$-5d and $4f^7$ states. In addition, recently another mechanism of thermally activated ionization from the $4f^6$5d to the conduction band is proposed to elucidate the thermal quenching behavior in the Eu^{2+} doped oxynitride $SrSi_2O_2N_2$ host with a rigid structure framework.[38] On the basis of the high quenching temperature and small stokes shift of the Eu^{2+} ion in the rigid $CaAlSiN_3$ host, the low thermal quenching effect is closely related to the thermally activated ionization. Of course, the small stokes shift derived low transition probability from the $4f^6$5d to the $4f^7$ state cannot be excluded.

Furthermore, as a nitride phosphor, the optimized $Ca_{0.98}Eu_{0.02}AlSiN_3$ shows excellent thermal and chemical stabilities. By the thermal gravity (TG) analysis up to 1000 °C (Figure 11), the oxidization of $Ca_{0.98}Eu_{0.02}AlSiN_3$ is found to occur at a temperature higher than 400 °C and then oxidized gradually to the corresponding $Ca_2Al_2SiO_7$ and SiO_2 (by XRD analysis). The weight increase is observed to be 19.2%, which is close to the stoichiometric value of 21.6% for the above two compounds. The high threshold of oxidization indicates that the $Ca_{0.98}Eu_{0.02}AlSiN_3$ is oxygen-resistant before 400 °C, which is much higher than the operating temperature of white LEDs. In addition, as shown in the inset of Figure 11, the emission intensity of $Ca_{0.98}Eu_{0.02}AlSiN_3$ is compared before and after soaking in 5 mol/L nitric acid for 72 h for the chemical stability test. After the acid soaking process, the intensity is slightly increased rather than decreased by acid corrosion, which means that the target phosphor is chemically stable in the ambient atmosphere. The slight increase of emission intensity may be contributed to removal of some acid-soluble impurities, such as the glass phase formed at high temperature.

For the potential application of this phosphor to the white LED illumination, the strong absorption in the range of 400−470 nm indicates that the $Ca_{1-x}Eu_xAlSiN_3$ phosphor can be efficiently excited by the blue light source of GaN and InGaN LEDs. The emission intensity of the optimized $Ca_{0.98}Eu_{0.02}AlSiN_3$ phosphor by SHS is compared with the $CaAlSiN_3$:Eu^{2+} sample prepared according to ref 13 (Mitsubishi Company provided) and commercially available YAG:Ce^{3+} (P46-Y3) standard. At the excitation of 460 nm, the intensity reaches about 95% of that prepared by solid-state reaction at high temperature and pressure and 120% of the YAG:Ce^{3+} standard. The CIE (Commission Internationale del'Eclairage) 1931 chromaticity index of this phosphor is (0.647, 0.347) which indicates the red emission of $Ca_{0.98}Eu_{0.02}AlSiN_3$ phosphor has high color saturation. Thus, this phosphor can be used to compensate the red color deficiency of YAG:Ce^{3+}-based white LEDs or to create white light by combining with a blue LED chip and another green phosphor.

(37) Kanou, T. *Handbook of Phosphors*; Ohm Press: Tokyo, 1987.
(38) Bachmann, V.; Jüstel, T.; Meijerink, A.; Ronda, C.; Schmidt, P. J. *J. Lumin.* **2006**, *121*, 441.

4. Conclusions

The efficient red phosphors, $CaAlSiN_3:Eu^{2+}$, have been successfully prepared by SHS from the CaAlSi intermetallic alloy precursor. The ignition occurs at 1050 °C, and further nitridation processes at higher temperature (1450−1550 °C) lead to the formation of $CaAlSiN_3:Eu^{2+}$ phosphors. The result of Rietveld refinement indicates the Eu^{2+} ions are tetrahedrally coordinated when they are incorporated into the host. Thus, the long emission is ascribed to the strong nephelauxetic effect in the rigid network and crystal field splitting in slightly distorted T_d symmetry. The sample doped with the Eu^{2+} ion at the optimized concentration of 2 atom % (vs Ca atom) is efficiently excited by the blue light (400−470 nm) and gives the red emission, peaking at 649 nm. The emission intensity exceeds (about 20%) that of the $YAG:Ce^{3+}$ (P46−Y3) standard at the same excitation of 460 nm. The post-annealing treatment results in the formation of vacancies on Ca sites and distortion of the crystal structure. The variation of photoluminescence properties is attributed to the change of the surrounding environment of Eu^{2+} ions. As a nitride phosphor, the optimized sample exhibits a low-temperature quenching effect, as well as excellent chemical and thermal stabilities. In addition, the saturated chromaticity index of (0.647, 0.347) also indicates that this efficient phosphor can be used as a potential candidate for the phosphor-converted white LEDs.

Acknowledgment. This work was partially supported by a Grant-in-Aid for the Scientific Research (No. 16080210) on Priority Areas (440) from the Ministry of Education, Culture, Sports, Science and Technology of Japan.

Note Added after ASAP Publication. There was an error in the Supporting Information file that accompanied the version of this paper that was published ASAP August 11, 2007; the correct Supporting Information file was published August 17, 2007.

Supporting Information Available: Photographs of as-prepared and annealed $Ca_{0.98}Eu_{0.02}AlSiN_3$ under UV light and under daylight (PDF). This material is available free of charge via the Internet at http://pubs.acs.org.

CM070623C